EVALUATION OF STABILITY OF A RESERVOIR EMBAMKMENT IN A HIGH SEISMIC ENVIROMENT

Faiz I. Makdisi[1], Zhi-Liang Wang[2] and Atta Yiadom[3]

[1] *Principal Engineer , AMEC Geomatrix, Inc., Oakland California, USA*
[2] *Senior Engineer , AMEC Geomatrix, Inc., Oakland California, USA*
[3] *Senior Civil Engineer, East Bay Municipal Utility District, Oakland, California, USA*
Emails: fmakdisi@geomatrix.com; zlwang@geomatrix.com; ayiadom@ebmud.com

ABSTRACT :

An effective-stress and non-linear approach was used for the seismic analyses of the Piedmont Reservoir embankment for a magnitude 7.5 design earthquake with peak acceleration of 0.7g. A plasticity constitutive model was used to simulate soil behavior. Computed performance was compared with observations during 1989 Loma Pieta earthquake. Analyses for the design earthquake indicated the potential for liquefaction and excessive deformation at the end of earthquake shaking.

KEYWORDS: Earth Embankment, High Seismicity Zone, Plasticity Model, Liquefaction.

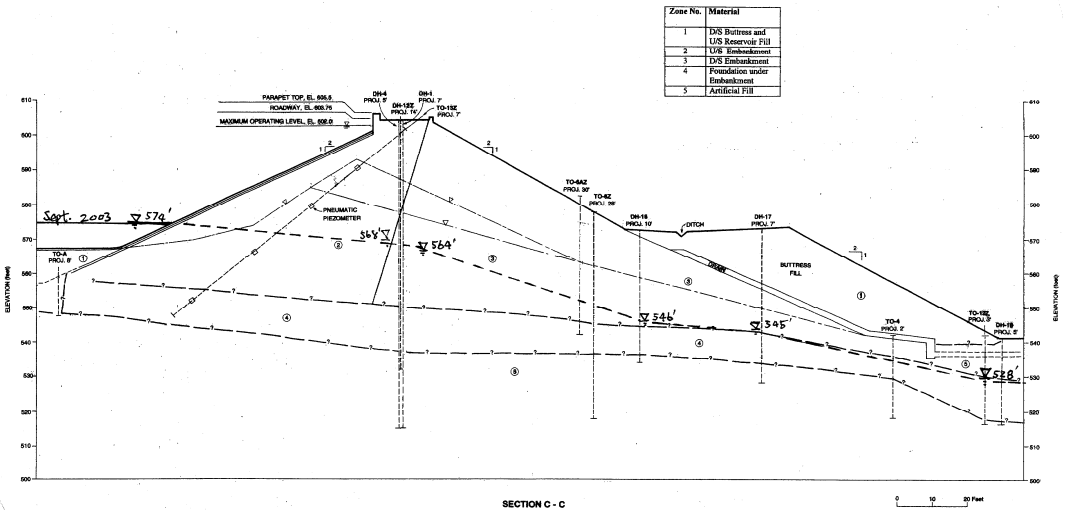

Figure 1 Maximum Cross Section of Piedmont Reservoir Embankment

1. INTRODUCTION

Piedmont Reservoir is an off-stream structure that provided water storage (about 24 million gallons). It was formed by placing an earth embankment about 60 feet high across a ravine. The embankment materials consist of compacted clayey to silty sands. Under the postulated magnitude 7.5 earthquake on the nearby Hayward fault, most zones of saturated sandy soils in the embankment and foundation likely would liquefy based on two-dimensional equivalent linear dynamic analyses. The downstream embankment slope likely would become unstable during or after the postulated earthquake shaking. In response to concerns about the seismic stability of the embankment, the reservoir water was restricted to a safe low level in September 2003. The lower part of the embankment and the underlying foundation colluvium, however remained saturated. It is conceivable that under the design earthquake shaking, the colluvium foundation and portions of the embankment below the phreatic surface could liquefy. Since there are operational structures within 40 feet of the downstream toe of the embankment, it was necessary to estimate how much deformation might be induced in the vicinity of the downstream toe during and after earthquake shaking. This

paper describes engineering analyses performed to estimate the earthquake-induced deformation at the maximum section of the Piedmont Reservoir embankment and its foundation in response to ground motions produced at the site.

2. EMBANKMENT SECTION AND MATERIAL PROPERTIES

The cross section is shown in Figure 1. The embankment was analyzed for a nearly empty reservoir level (at about elevation +574 feet). The materials comprising the embankment and foundation consisted of three soil types: (1) the embankment soils are classified as compacted clayey to silty sands; (2) the natural foundation colluvium is classified as more clayey than the embankment soils; (3) the bedrock underlying the colluvium foundation consists of highly weathered Franciscan Formation. The phreatic surface in the embankment was estimated based on measurements in piezometers.

Shear wave velocities were measured within the embankment and foundation materials using a cross-hole geophysical survey in borings drilled through the embankment. The dynamic shear modulus of the soil, G_{max}, is related to the shear wave velocity by the following relationships: $G_{max} = \rho(Vs)$, where Vs is the shear wave velocity, and ρ is the mass density. Studies by Seed and Idriss (1970) showed that the dynamic shear modulus of granular soils is related to the effective confining pressure as follows:

$$G_{\max} = 1000\, K_{2\max} (\sigma_m')^{1/2}, in\ psf \qquad (1)$$

where: K_{2max} = parameter relating G_{max} and σ_m' and a function of density or void ratio
σ_m' = mean effective confining pressure in psf

The field measured shear wave velocity values were used to estimate the K_{2max} parameters for the embankment and foundation soils at various depths. The soil parameters used in the analyses are summarized in Table 1. Site-specific modulus reduction and damping relationships with shear strain were used to calibrate model parameters.

Table 1 material zones and properties

Zone No.	Zone Description	Selected $(N_1)_{60\text{-}cs}$	ϕ′ degrees	C' (psf)	Moist Unit Weight (pcf)	Saturated Unit Weight (pcf)	K_{2max}
I	D/S Buttress and U/S Res. Fill	20	36	0	130	130	70
II	U/S Embankment	20	36	0	129	133	65
III	D/S Embankment	20	36	0	131	133	43
IV	Foundation under Embankment	20	35	0	128	133	65
V	D/S Artificial Fill	20	37	0	123	133	65

Notes: D/S = downstream, U/S = upstream

3. SOIL MODEL AND PARAMETERS FOR EFFECTIVE-STRESS ANALYSIS

A comprehensive yet practical constitutive model for sand (Wang et al., 1990) was developed within the general framework of bounding surface plasticity. To implement the model into the computer code FLAC (Itasca, 2000), formulations were derived that conform to plane-strain conditions (Wang and Makdisi, 1999). This version retains the capability of simulating the generation of pore water pressure and soil liquefaction. Figure 2 shows the failure surface, maximum pre-stress surface, and phase transformation line. These definitions are plotted in terms of effective mean stress, p, and the second deviatoric stress invariant, J. Eight parameters are required to perform an effective-stress analysis using the model. Three of the parameters (ϕ, G_o, and h_r) can be estimated from parameters

used in the equivalent-linear approach; two parameters (k_r and d) can be calibrated based on cyclic strength data from laboratory tests or from field standard penetration test (SPT) results; the parameter ν, is Poisson's ratio; and the last two parameters (b and R_f/R_f) can be estimated or calibrated using monotonic undrained test results.

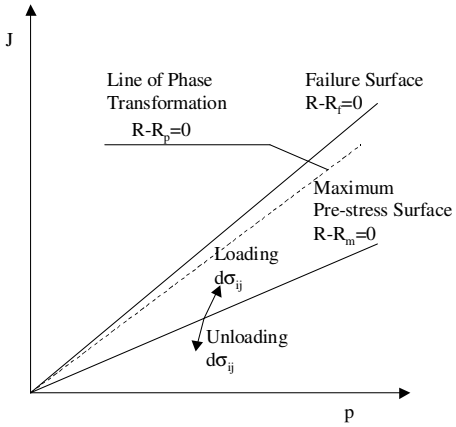

Figure 2(a) Surfaces and stress variables in J-p plane

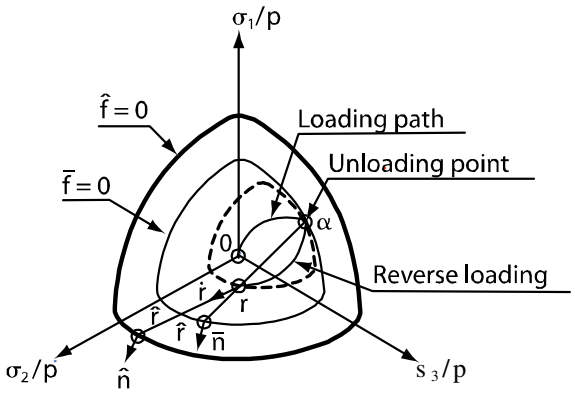

(b) Surfaces and stress variables in p = constant plane

Parameter ϕ is the effective friction angle.

Parameter G_o is the modulus coefficient that defines the initial (maximum) elastic shear modulus, G_{max}, using the following equation:

$$G_{\max} = G_o p_a V(e)\sqrt{\frac{p}{p_a}} \quad , \quad V(e) = \frac{(2.973-e)^2}{1+e} \tag{2}$$

where p_a is the atmospheric pressure, e is the void ratio, and p is the mean effective confining pressure. The model parameter G_o can be related to the value K_{2max} by:

$$G_o = 21.738 K_{2\max} / V(e) \tag{3}$$

Parameter h_r characterizes the nonlinear relationship between shear modulus and shear-strain amplitude. For the Piedmont Reservoir embankment, site-specific modulus reduction curves were used to calibrate the model parameter h_r.

Parameters k_r, which affects the changes in effective stress under monotonic (and virgin) loading conditions, was calibrated using the results of monotonic laboratory test results. For the material in the unsaturated zone, a value of k_r = 100 was used to eliminate the generation of excess pore water pressure and liquefaction.

Parameter b is used to vary the shape of the effective-stress path in the model simulation. A default value of 2 often is used, and was used here.

Parameter d is calibrated based on the cyclic resistance of the soil. The cyclic strength of sandy soils is defined as the cyclic stress ratio that would cause pore pressure buildup and liquefaction in a specified number of cycles. In this study, cyclic strength was estimated based on in situ SPT data and observed performance during earthquakes. The empirical relationship shown on Figure 3 (Seed et al., 1985; Youd and Idriss, 1997) relates the cyclic stress ratio causing liquefaction to the standard penetration resistance [$(N_1)_{60}$] value for a magnitude 7.5 earthquake. In addition to the relationship for a magnitude 7.5 earthquake**,** relationships also were developed for scaling for magnitude effects and for relating earthquake magnitude to an equivalent number of uniform stress cycles in laboratory tests. Based on these data, a relationship between cyclic stress ratio and number of cycles to liquefaction was developed for several $(N_1)_{60}$ blow counts (see Figure 5). In this figure the stress ratio is presented in terms of the shear stress divided by mean effective stress (τ/σ_{m0}'), assuming K_o = 0.5.

Model parameter d controls the development of excess pore water pressure due to cyclic loading under undrained conditions. The number of cycles required to cause liquefaction of a soil element was estimated based on the

computed effective-stress path (or shear stress vs. effective mean pressure), as shown on Figure 4 for a given cyclic stress. From the example presented in Figure 4, (for parameters $k_r = 1.5$ and $d = 5.5$) at a specified stress ratio of 0.4, eight cycles are needed to reduce the mean effective pressure to the point of triggering liquefaction. For characterizing liquefaction resistance of the embankment and colluvium foundation materials, an average fines-corrected $(N_1)_{60\text{-cs}}$ blow count of 20 (HTA, 2003) was selected for calibrating model parameters. The model simulation (for $(N_1)_{60\text{-cs}}$ of 20) using the above specified model parameters is shown in dashed line on Figure 5, and is compared with cyclic strength curve from the field data.

Parameter ν is the Poisson's ratio. An estimated value of 0.3 was used for all materials.

Parameter R_p represents the so-called phase transformation line. It was estimated from laboratory test results. For this study, $R_p/R_f = 0.7$ was used.

Model parameters assigned to the materials in the cross section analyzed for this study are presented in Table 2.

Table 2 material zones and model parameters

Zone No.	Void ratio	ϕ′	G_o	ν	h_r	k_r	d	R_p/R_f	b
I	0.56	36	407	0.3	0.18 to 0.47	1.5	5.5	0.7	2.0
II	0.50	36	345	0.3	0.18 to 0.47	1.5	5.5	0.7	2.0
III	0.50	36	228	0.3	0.18 to 0.47	1.5	5.5	0.7	2.0
IV	0.50	35	345	0.3	0.18 to 0.47	1.5	5.5	0.7	2.0
V	0.50	37	345	0.3	0.18 to 0.47	1.5	5.5	0.7	2.0

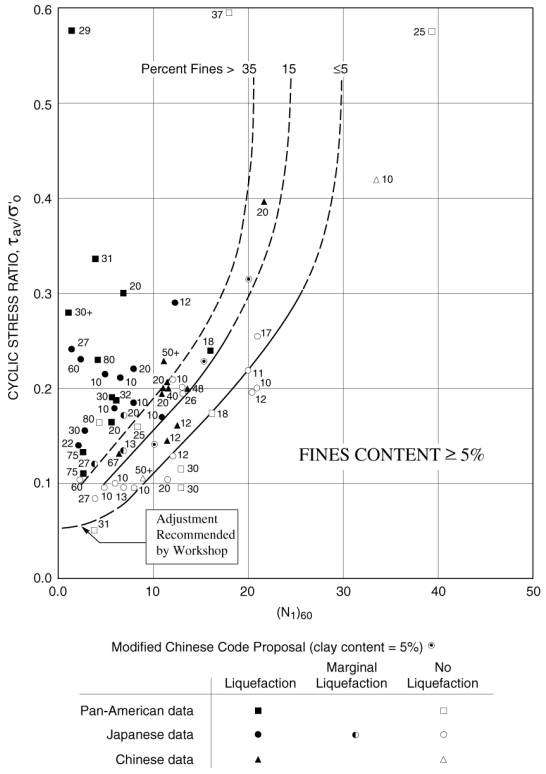

Figure 3 Relationship between cyclic stress ratio causing liquefaction and $(N_1)_{60}$ values for M_w= 7.5 earthquakes

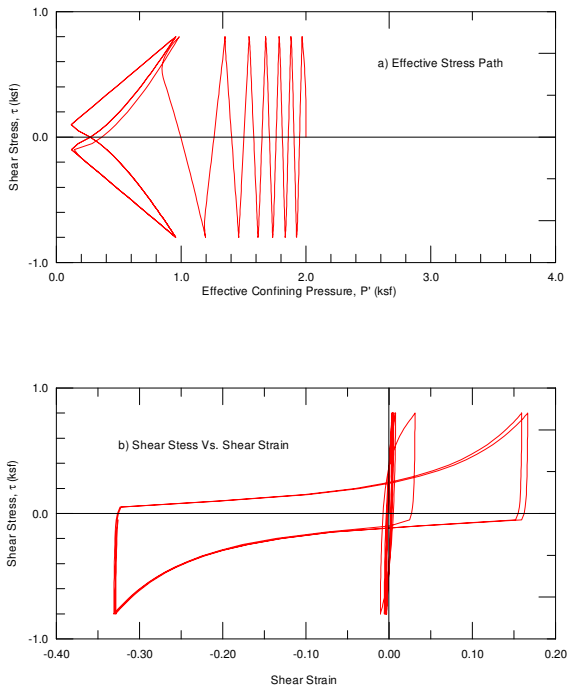

Figure 4 Computed cyclic stress-strain relations for stress ratio=0.40

4. STATIC STRESS AND SEEPAGE ANALYSES

A finite-difference grid (shown on Figure 6) was developed to represent the maximum cross section shown on Figure 1. The concrete facing material was not simulated in this analysis. Static stresses within the various embankment zones were computed using a layer-by-layer procedure that simulates the construction of the embankment. The effect of the reservoir water was then simulated in three steps. First, water pressure as a pressure load was applied to the upstream slope. Second, seepage analysis was performed to develop a phreatic surface in the embankment. Third, the static stresses were recalculated considering the effects of the pore water pressure and seepage forces developed in the embankment.

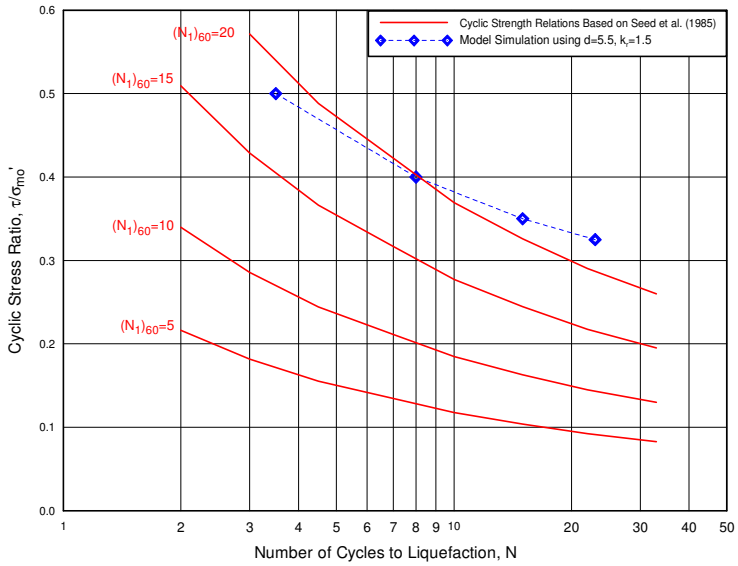

Figure 5 Cyclic strength relations compared to model simulations

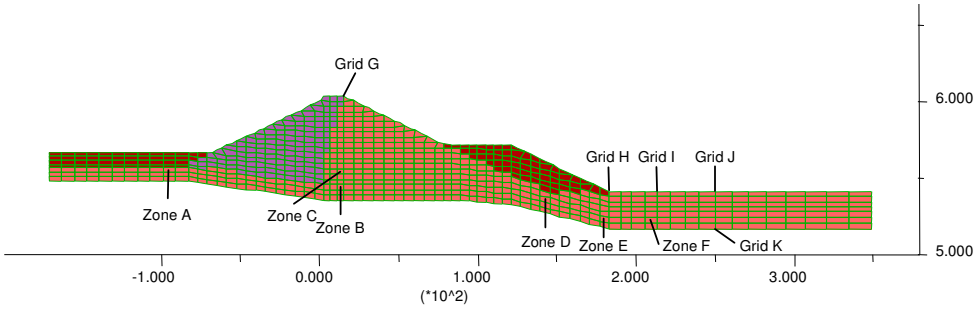

Figure 6 Material zones and finite-difference grid (ft.), maximum geotechnical cross-section

5. DYNAMIC EFFECTIVE-STRESS ANALYSES

Dynamic effective-stress analyses were performed for the maximum section of the Piedmont Reservoir embankment under "empty" reservoir conditions, given the design ground motions postulated for the site.

5.1. Dynamic Properties and Boundary Conditions

A rock input motion was applied at the base of the finite-difference model shown in Figure 6. The ground motion

record corresponds to an earthquake having a magnitude 7.5 and occurring on the nearby Hayward fault with estimated peak acceleration about 0.7g and an estimated peak velocity of about 80 cm per second. Time histories (acceleration, velocity, and displacement) of the ground motion record are presented on Figure 7. Because we employed the rigid base option in this analysis, we applied a revised input motion at the base of the finite-difference grid. Using the program SHAKE and the above design motion to first develop an interface motion under the downstream free field having an assumed average shear wave velocity of 2,500 feet/second for the bedrock. The right and left boundaries of the model were simulated using two viscous free-field boundaries, allowing wave propagation through these boundaries in the horizontal direction. The parameters for the user-defined plasticity model were described earlier and presented in Table 2.

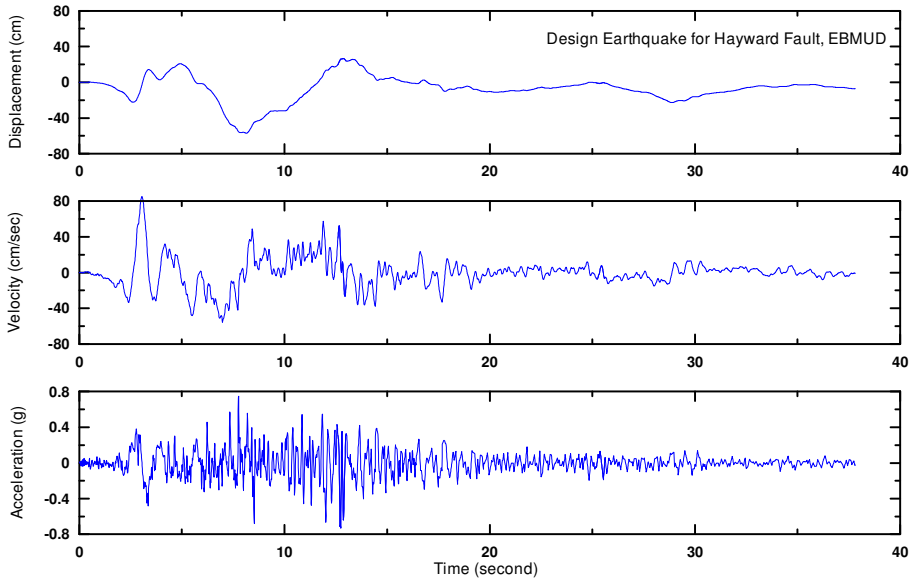

Figure 7 Design input rock motion for a M7.5 event

5.2 Results of Dynamic Analyses

The dynamic finite-difference analysis provides the acceleration response at each of the grid points in the model. The computed acceleration time histories at the crest of the embankment and at the free field (about 50 feet beyond the downstream toe) indicate that the input motion has propagated to the crest of the dam for approximately the first 4 seconds. As discussed below, the saturated zones within the embankment and foundation were estimated to liquefy after about 5 seconds of shaking. The crest and free-field responses for the remaining 35 seconds of shaking indicate a significant reduction in the level of shaking compared to the input acceleration at the base of the grid.

Time histories of effective mean confining pressure computed for six zones in the saturated embankment and foundation colluvium are presented on Figure 8. Liquefaction occurred (after about 4 seconds of shaking), first at both the upstream and downstream free field locations (zone A, E and F in Figure 6), then extended to locations beneath the crest (zones B and C) and the beneath the downstream buttress (zone D) at about 8 seconds, following the onset of the peak acceleration pulse of 0.7g in the input motion.

The predicted deformed shape of the embankment and foundation at the end of earthquake shaking is shown on Figure 9. This figure shows that at the end of earthquake shaking, the computed maximum settlement at the crest is about 17 feet. Maximum computed horizontal displacements on the downstream slope were about 27 feet. The time histories of horizontal displacements at several grid points (shown in Figure 7) are presented in Figure 10. The point on the downstream toe of the embankment (grid point H) shows a maximum displacement at the end of earthquake shaking of about 23 feet.

In the free field downstream of the toe of the embankment, where the existing structures are located, the maximum

computed horizontal displacement is in the range of 15 to 20 feet. This level of displacement was judged to adversely impact the existing structures located about 40 feet from the toe of the embankment.

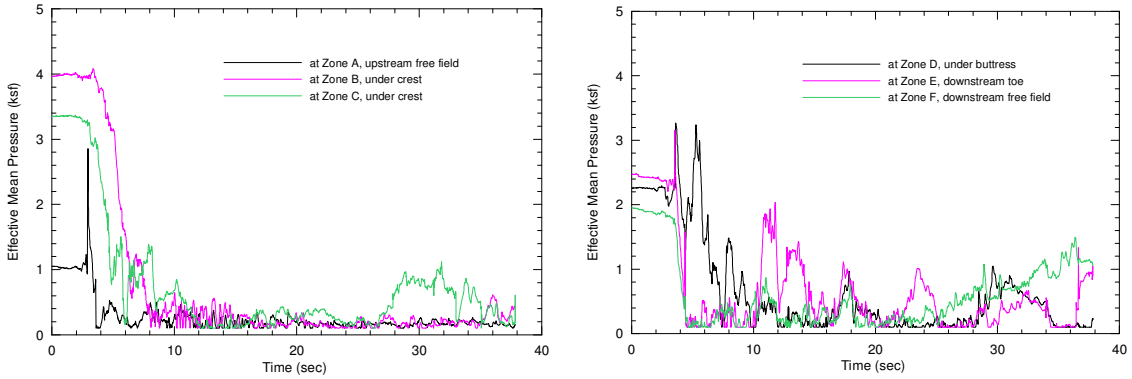

Figure 8 Computed effective mean pressure time histories in saturated zone

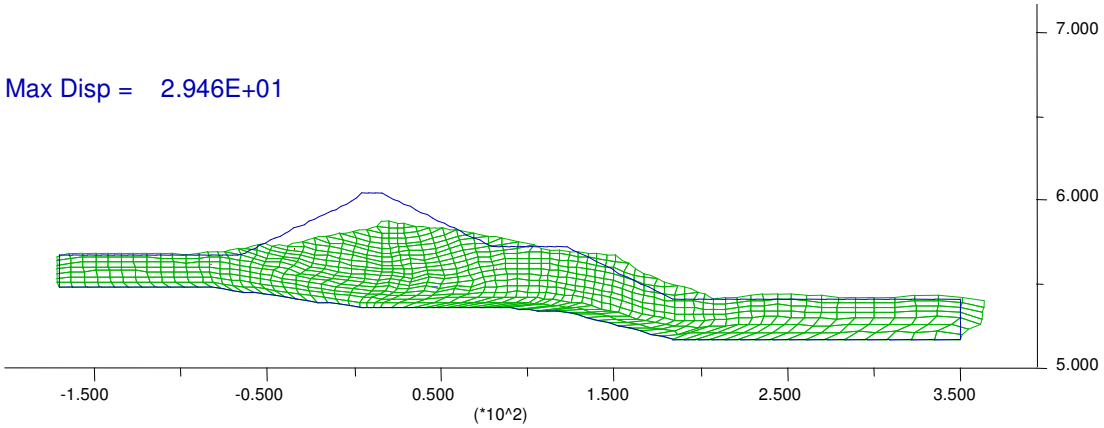

Figure 9 Computed deformed grids (ft) of the embankment after earthquake shaking

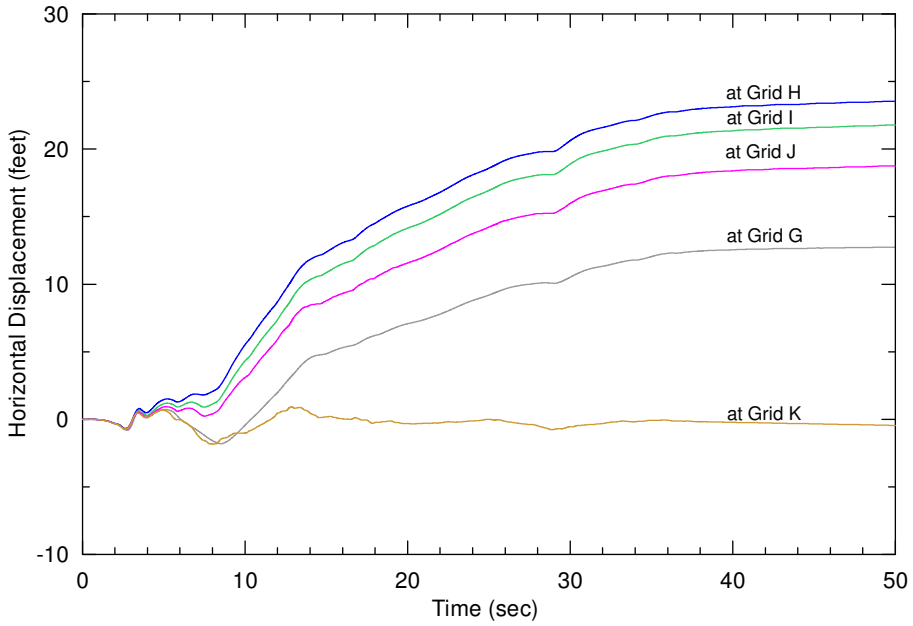

Figure 10 Computed horizontal displacement time histories

5.3 Verification of Results of Dynamic Analyses

The observed performance of the reservoir embankment during the Loma Prieta, California earthquake of October 17, 1989 was used to verify the results of the dynamic analysis procedure described in this study. A survey by the dam owner showed no observable deformation after the earthquake. The FLAC analysis was performed for the full reservoir level reported to have existed during the Loma Prieta earthquake. A time history of rock motions, recorded during the earthquake and located about 1 km from Piedmont Reservoir, was used as input motion for the analysis.As stated earlier, the concrete lining at the upstream face of the embankment was not modeled in this analysis. The predicted deformation by this analysis indicated a horizontal crest displacement of 0.4 inches, and vertical settlement of about 2.4 inches. These results indicate that the analyses predicted horizontal deformations that were in reasonable agreement with the observed performance, however, analysis over predicted the crest settlement. This was attributed to the fact that the concrete lining that covers the upstream slope was not modeled in the analysis. Accordingly the results of the current analysis were judged to be conservative.

6. SUMMARY AND CONCLUSIONS

A coupled, nonlinear effective-stress approach was used to perform deformation analyses of the maximum cross section of the Piedmont Reservoir embankment for an "empty" reservoir condition. In the effective-stress analyses, plasticity model parameters were calibrated using laboratory test results, measurements of shear wave velocity, representative standard penetration test blow counts [$(N_1)_{60}$], and the liquefaction resistance chart of Seed et al. (1985), as updated in Youd and Idriss (1997).

For the embankment material and colluvium underlying the embankment, an average fines-corrected $(N_1)_{60}$ value of 20 blows per foot (based on field SPT data) was used for the analysis. Static stress and seepage analyses were performed prior to the dynamic analysis. A time-history having a peak ground acceleration of 0.7g was used as input in the dynamic analysis. Pore water pressure and mean effective-stress time histories computed for the foundation indicate that liquefaction would occur after about 4 seconds of shaking. Computed permanent displacements show significant movements (about 20 to 30 feet of horizontal movement) in the downstream slopes of the embankment. In the free field beyond the downstream toe, computed displacements in the range of 15 to 20 feet were judged to impact the structures in the vicinity. The analyses described in this paper are finding increased applications and becoming a useful tool in practical earthquake engineering problems (Wang et al, 2006).

7. REFERENCES

Harlan Tait Associates. (2003). Seismic Stability of Piedmont Reservoir Embankment, October 22.

Itasca. (2000). FLAC, Fast Lagrangian Analysis of Continua, Version 4.0, User's Guide: Itasca Consulting Group, Inc., Thrasher Square East, 708 South Third Street, Suite 310, Minneapolis, Minnesota.

Seed, H.B., and Idriss, I.M. (1970). Soil moduli and damping factors for dynamic response analyses: Earthquake Engineering Research Center, University of California, Berkeley, Report No. EERC 70-10.

Seed, H.B., Tokimatsu, K., Harder, L.F., and Chung, R.M. (1985). Influence of SPT procedures in soil liquefaction resistance evaluations: *Journal of the Geotechnical Engineering Division*, American Society of Civil Engineers, **111:12**. 1425-1445.

Wang, Z.L., Dafalias, Y.F., and Shen, C.K. (1990). Bounding surface hypoplasticity model for sand. *Journal of Engineering Mechanics,* American Society of Civil Engineers. **116:5**. 983-1001.

Wang, Z.L., and Makdisi, F.I. (1999). Implementing a bounding surface hypoplasticity model for sand into the FLAC program. in Detournay, C., and Hart, R. (eds.), FLAC and Numerical Modeling in Geomechanics: A.A. Balkema, Netherlands, p. 483-490.

Wang, Z.L., Makdisi, F.I. & Egan, J. (2006). Practical Applications of a Non-linear Approach to Analysis of Earthquake-Induced Liquefaction and Deformation of Earth Structures. *Journal of Soil Dynamics & Earthquake Engineering,* **26 (2-4)**: 231-252.

Youd, T.L., and Idriss, I.M. (eds.), 1997, Proceedings of the NCEER Workshop on Evaluation of Liquefaction Resistance of Soils: National Center for Earthquake Engineering Research, Technical Report NCEER-97-0022, December 31, 276 p.